

High Energy Nuclear Collisions

K. J. Eskola

Department of Physics, University of Jyväskylä, P.O. Box 35, FIN-40351 Jyväskylä,
 Finland

E-mail: kari.eskola@phys.jyu.fi

Abstract

Highlights of the results from ultrarelativistic heavy ion collisions at CERN-SPS are reviewed. In particular, I discuss how the experimental results indicate that a collective strongly interacting system has been produced, and what are the implications towards the Quark Gluon Plasma. The physical ideas behind measuring certain observables are introduced. The future program of high energy nuclear collisions at BNL-RHIC and CERN-LHC/ALICE is also briefly discussed.

Plenary talk at the International Europhysics Conference on High Energy Physics, EPS-HEP99, Tampere, Finland, July 1999.

1. Introduction

This talk is organized as follows: In the first, introductory section, I will briefly recapitulate the physics motivations for colliding heavy ions at ultrarelativistic energies. For the second section, I have selected some of the experimental highlights from ultrarelativistic heavy ion collisions (let me use an acronym URHIC) at CERN-SPS. For each topic, the basic idea will be explained first, followed then by a discussion of the interesting experimental observations. As URHIC at the SPS represent the highest energy nuclear collisions so far, they and their implications will have the main emphasis in this review. In the third section, I will briefly discuss the future program for heavy ions, BNL-RHIC and the ALICE experiment at CERN-LHC. In the fourth section, I will present my conclusions. For recent reviews on the same subject, see e.g. [1, 2, 3, 4].

1.1. General facts

The main goal of ultrarelativistic heavy ion collisions is to study the thermodynamics of strongly interacting matter. In colliding two heavy nuclei ($A \sim 200$) together at very high cms energies ($\sqrt{s} \sim 20 \dots 200 \dots 5500$ AGeV), the primary aim is to produce experimentally a new phase of matter, the Quark-Gluon Plasma (QGP), and – even more importantly – to *observe* the QCD phase transition from the QGP phase to the Hadron Gas (HG) phase. Cosmological motivation for URHIC is the fact that our Universe has undergone such a transition within its first microseconds.

In general, although the basic motivation for such studies comes from the theory, it is fair to state that the field of URHIC is an experimentally driven one. In this field, it is very difficult to perform calculations from first principles, so – in addition to precision measurements – good, QCD-based phenomenology is needed.

In relation to conventional high energy particle physics (HEPP), URHIC naturally share the goal of making high precision measurements. However, the two fields are orthogonal with respect to their physics goals: where HEPP aims for detection of new particles and new symmetries (Higgs, SuSy), URHIC reach for detection of a new phase of matter, made of the known QCD-quanta. In HEPP, simplicity is obtained through producing as *few* particles in the final state as possible, whereas in URHIC simplicity is obtained by producing as *many* particles in the final state as possible: only if the strongly interacting system becomes dense and large enough it can become collective and laws of thermodynamics become applicable. In other words, for URHIC the goal is to do elementary particle condensed matter physics. In this, and throughout my talk as well, the keywords are *lifetime* and *volume* of the produced, extended, system.

1.2. QCD phase diagrams

The theoretical foundation for searching the new QCD-phase of matter is given by the first principles calculations of lattice-QCD (for a review, see [5]). From there we know that the QGP phase with

partonic degrees of freedom undoubtedly exists. An example of these calculations for the Equation of State (EoS, pressure as a function of energy density) of the QCD-matter is given in Fig. 1. The abrupt change in the energy density from the confined phase at low T to the deconfined phase at high T is a consequence of a first order phase transition in the pure gauge $SU(3)$. With dynamical fermions but still with zero baryochemical potential $\mu_B = 0$ (which corresponds to zero net baryon number), the order of the phase transition has been seen to change with the number of quark flavours and with masses of the three lightest quarks. For the moment, inclusion of dynamical fermions can only be done in certain approximations and keeping $\mu_B = 0$. Calculations with $\mu_B \neq 0$ are not yet available, due to the complex valued actions.

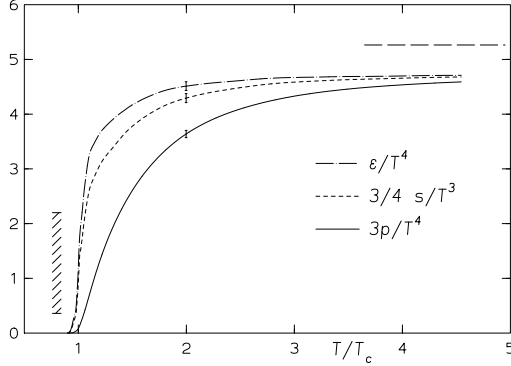


Figure 1. Scaled energy density, entropy density and pressure vs. scaled temperature at the continuum limit in pure gauge $SU(3)$ theory [6, 5]. The horizontal dashed line is the ideal gas limit and the vertical hatched band illustrates the latent heat. The figure is from [6].

The critical deconfinement temperature T_c at $\mu_B = 0$ is about 265 MeV for the pure $SU(3)$ glue, with quarks the estimates lie in the region $T_c = 140...200$ MeV [5]. While the deconfinement phase transition is studied through Polyakov loops, the phase transition related to chiral symmetry can be studied through chiral condensates $\langle \bar{\Psi}\Psi \rangle$. In the lattice QCD calculations, chiral symmetry has been observed to be restored (i.e. $\langle \bar{\Psi}\Psi \rangle \rightarrow 0$) always at the same T_c as the deconfinement transition occurs [5].

With URHIC, one explores the QCD phase diagram in the μ_B, T -plane as illustrated in Fig. 2. With increasing nuclear mass number A and with increasing cms-energy, more partons are liberated in the collision and the energy density of the initial QGP-system (immediately after the AA-collision) increases. With increasing initial energy densities

and increasing initial temperatures, sketched by the arrows in Fig. 2, the lifetime and the volume of the plasma evidently increase as well, improving the chances for observing signals directly from the QGP. Baryon stopping has already been observed to decrease with the cms-energies [7], and this trend is expected to continue at larger \sqrt{s} . With less net baryon number stopped in the central rapidity region, which is the main region of interest for the QGP studies, also μ_B will decrease, as illustrated in the figure. Ideally, it would of course be beneficial to get as close as possible to the theoretically best understood limit $\mu_B/T \rightarrow 0$. Cosmologically, the interest lies also in this region: in the early Universe, the inverse of the specific entropy is tiny, $\sim 10^{-9}$.

At very high cms-energies, the formed QGP can be said to be produced by “heating”: the QGP consists of gluons and quark-antiquark pairs, and the energy for creating them is provided by the high cms-energy. The QGP can exist also at $T = 0$ at large values of μ_B . This would correspond to preparing the QGP by compressing the normal nuclear matter beyond the critical density, which is of the order of ~ 10 times the normal nuclear matter density 0.17 fm^{-3} . This may happen in the cores of neutron stars but as this region is not relevant for URHIC, I will not discuss it here.

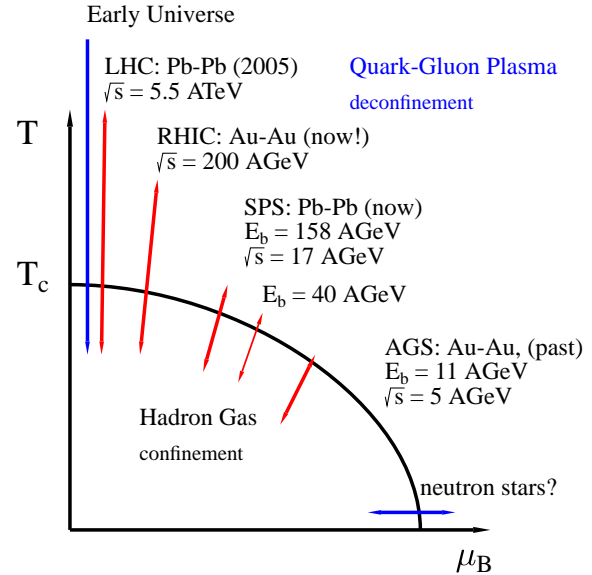


Figure 2. An illustration of the conventional QCD phase diagram in the plane of chemical potential μ_B and temperature T . The regions of the phase diagram the highest energy heavy ion collisions are probing are sketched by the arrows.

The current and future experimental program of highest energy nuclear collisions is also illustrated

in Fig. 2. In addition to the experiments I will discuss below, also an extensive intermediate and lower energy program for heavy ions (BNL-AGS, GSI-SIS, etc.) exists but in this talk I will concentrate only on the highest energy collisions. In the fixed target experiments at the Super Proton Synchrotron (SPS) of CERN, the highest beam energies have been $E_b = 200 \text{ AGeV}$ for ^{32}S , and currently $E_b = 158 \text{ AGeV}$ for the Pb-beam in $^{208}\text{Pb}+^{208}\text{Pb}$ collisions. The corresponding nucleon-nucleon cms-energies are $\sqrt{s} = 20 \text{ GeV}$ and 17.3 GeV . A lower energy run at the SPS with $E_b = 40 \text{ AGeV}$ will take place this year. In the near future, starting in December 1999, in the Relativistic Heavy Ion Collider (RHIC) at the Brookhaven National Laboratory (BNL), the collisions of highest energy and heaviest nuclei will be $^{197}\text{Au}+^{197}\text{Au}$ at $\sqrt{s} = 200 \text{ AGeV}$. In year 2005, in A Large Ion Collider Experiment (ALICE) at the Large Hadron Collider (LHC) at CERN, one will collide ^{208}Pb nuclei on ^{208}Pb at $\sqrt{s} = 5500 \text{ AGeV}$.

As it is expected that baryon stopping nearly vanishes at the LHC energies, the experimental URHIC program will probe an extensive range of the conventional QCD phase diagram in the μ_B, T -plane. The critical question is whether the QCD phase transition can indeed be observed. Regarding the QCD phase diagram itself, there have been very interesting theoretical developments recently: at high densities, quarks may form Cooper pairs and a new, color superconducting, phase may exist [8, 9, 10]. Most probably this happens at larger values of μ_B than will be reachable experimentally by URHIC. On the other hand, the μ_B, T -phase diagram may have a critical or tricritical point somewhere along the phase transition line in Fig. 2, depending on the order of the phase transition in full QCD – which depends on the masses of dynamical quarks and the effects of finite μ_B . By varying the cms energy it may be possible to trace this point down. For a recent review of these exciting theoretical developments, see [10].

1.3. Space-time evolution: lifetime and volume

The basic difference between URHIC and collisions of point-like (e^+e^-) or small composite particles ($p+\bar{p}$, $p+p$) is that an ideal system produced in URHIC is an extended and collective one with a large volume and a long lifetime. Once the system is produced, its space-time evolution cannot be controlled. In fact, the only experimentally controllable initial parameters are the mass numbers of the colliding nuclei and the collision energy. In addition, a handle on the impact parameter in each collision can be obtained by

forming event classes of different multiplicities and transverse energies with a correlation to the energies observed in the zero-degree calorimeter. With these few controllable initial parameters, information of the whole space-time evolution of the system must be extracted from the various observables measured in the final state.

The different stages in the space-time evolution of a strongly interacting system produced in an URHIC can be pictured as in Fig. 3. At sufficiently high energies, the colliding nuclei are Lorentz-contracted thin disks surrounded by virtual clouds of partons. The original impact of the nuclear disks takes place almost instantaneously (within a transit time $\tau_{\text{tr}} = 2R_A/\gamma$) in a region around $z, t \sim 0$. Primary production of gluons, quarks and antiquarks occurs in the central rapidity region during some typical formation time τ_0 of the order of a fraction of fm/c, and $\tau_{\text{tr}} \ll \tau_0$. In a dense enough system the mean free paths of the QCD-quanta are much less than any typical homogeneity size V in the system: $\lambda_{\text{mfp}}^3 \ll V$. A dense enough system reaches quickly a *kinetic* equilibrium with *locally* thermal quark and gluon momentum distributions. *Chemical* equilibration is preferable but not necessary to define a QGP, i.e. the density of quarks and antiquarks relative to that of gluons does not need to coincide with that in an ideal gas. The system will further evolve collectively as a QGP if it is interacting strongly enough and if the scattering times of quarks and gluons are much less than the inverse of the expansion rate (Hubble constant⁻¹) of the system. For a recent discussion, see e.g. [1].

In the most ideal case – in the limit of a very dense system – the evolution of the system after its formation can be described in terms of hydrodynamics. If the system were exactly longitudinally boost invariant, physics would be invariant along hyperbolas of constant longitudinal proper time $\tau = \sqrt{t^2 - z^2}$ [11]. In reality, however, already due to its edges the system is never perfectly boost invariant, which is illustrated in Fig. 3 by the curves bending backwards in time near the light cones. Notice also that depending on baryon stopping the temperatures and chemical potentials in the central rapidity region can be quite different from the ones at large rapidities.

Analogously to the early Universe in the Big Bang cosmology, the produced QGP system expands and cools. Eventually the system ends up in a Hadron Gas phase. If the QCD-phase transition is of first order, a stage of a mixed phase with both QGP and HG coexisting at a (local) critical temperature and chemical potential will appear in between. In the end of the HG phase,

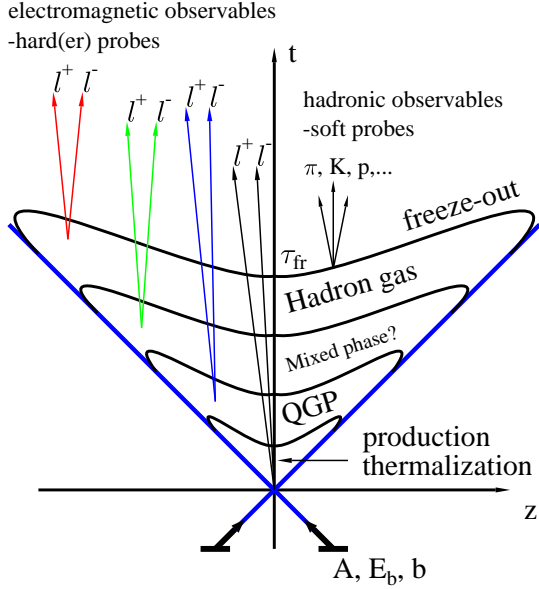


Figure 3. Space-time evolution of a strongly interacting system produced in a very high energy $A+A$ collision, projected in the plane of the longitudinal coordinate z and time t . Different stages of evolution and different types of observables are demonstrated.

the average mean free paths of hadrons exceed the homogeneity size of the system, $\lambda_{\text{mfp}}^3 > V$, and the Hadron Gas decouples, i.e. freezes out. The hydrodynamical, locally thermal, picture ceases to apply at this point. In terms of hydrodynamics, the final state hadrons are emitted from the freeze-out surface. Notice, however, that the decoupling does not take place instantaneously: as illustrated in Fig. 3, due to Lorentz-dilation effects, the regions near light cones freeze out typically later than the central regions. Furthermore, even within a certain spatial region decoupling is never an instantaneous process (as drawn in the figure for simplicity) but a dynamical one, determined by the expansion rate and the hadronic rescattering cross sections.

The probes of strongly interacting matter can be divided into hadronic and electromagnetic ones. Typically, as illustrated in Fig. 3 the hadronic probes reflect the conditions at the freeze-out hypersurface, i.e. at the very last stage of the collective evolution. The electromagnetic probes, thermal lepton pairs and photons [12,13,14], in turn are emitted throughout the whole space-time history of the system; they decouple immediately due to their long mean free paths. The thermal electromagnetic probes have to compete with the primary production processes, e.g. Drell-Yan process for dileptons and prompt photon production for photons, which have the same origin in hard

scatterings as in hadron-hadron collisions. Also the hadrons emitted from the freeze-out surface may decay electromagnetically and contribute strongly to the background for the electromagnetic probes. Because of the rapidly falling exponential momentum distributions in the thermal system, the momentum or mass scale of an electromagnetic probe is typically close to the local temperature at the time of emission. Therefore, the harder the probes are, the hotter and earlier system they typically probe. The probes coming directly from hard scatterings in the primary nuclear collision are the earliest ones and usually referred to as “hard probes” [15]. Some hard probes, like jet production (also in connection with direct photons) are strongly interacting but – thanks to the large momentum or mass scale $Q \gg T$ involved – they are not absorbed in the QGP or HG.

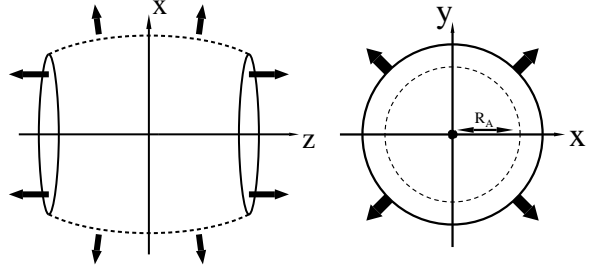


Figure 4. Snapshots of an expanding system in longitudinal-transverse coordinate z, x -plane, and in transverse coordinate x, y -plane. The black arrows indicate the longitudinal and transverse flow. The rest frame radius of a nucleus A is denoted by R_A .

At very high energies, in a first approximation the produced system expands only longitudinally [11]. If the colliding nuclei were transversally infinite disks, this would be the case because no pressure gradients would be generated in the transverse direction. In reality, however, the colliding nuclei have rapidly falling nuclear density distributions (“edges”), and pressure gradients in the transverse direction are generated in the production and thermalization stage. Then, if the lifetime of the collective system is long enough, a strong transverse expansion develops [16]. Consequently, at freeze-out the transverse size of the system can become clearly larger than the original nuclear radius $R_A \sim 7$ fm for $A \sim 200$. This is illustrated in Figs. 4. The quantitative details of evolution of the transverse flow depend on the actual densities and pressure gradients generated in the very beginning of the QGP phase, and on the actual EoS in the locally thermal system. The z, x -projection in Fig. 4 demonstrates the longitudinal

and the transverse flow. Notice here that at a fixed time t the different spatial regions in z are at different stages of the evolution, as illustrated by Fig. 3.

2. Highlights from the SPS

In this section, I have picked up some of the highlights of the experimental results from URHIC at the SPS. I will concentrate on the observations that make URHIC very different from hadron-hadron collisions. In particular, I will discuss the experimental evidence of collective behaviour of strongly interacting matter. I will briefly review the anomalies observed in URHIC at the SPS: the strangeness enhancement from WA97, the low-mass dielectron enhancement from CERES/NA45, and the J/Ψ -suppression from NA50, and discuss the physics implications of these experimental facts.

2.1. Transverse flow

As discussed in the previous section, if the lifetime of the produced collective system is long enough, a strong transverse flow is generated. At freeze-out, the system emits particles from its decoupling surface according to the appropriate thermal distributions at each *local* freeze-out temperature T_{fo} and baryochemical potential μ_B^{fo} . These distributions, however, must be folded with the (local) flow velocity in each emitting cell. Since the flow is a collective phenomenon, particles of different masses obtain the same velocity from it, and consequently the heavier the particle is the more transverse momentum it gains from the transverse flow. The collective transverse flow \mathbf{v}_T obviously therefore makes the transverse momentum spectra of heavier final state hadrons flatter than those of the lighter hadrons. In the m_T -distributions $dN/dm_T^2 \sim \exp[-m_T/T_{slope}]$, the inverse slope parameter T_{slope} can be expressed as

$$T_{slope} = T_{fo} + \frac{1}{2}m\langle v_T^2 \rangle \quad (1)$$

at the nonrelativistic domain $p_T \ll m$ and as a “blueshift” formula

$$T_{slope} = T_{fo} \sqrt{\frac{1 + \langle v_T \rangle}{1 - \langle v_T \rangle}} \quad (2)$$

at the relativistic region $p_T \gg m$ [17].

In Fig. 5 [18,19], also shown by Helstrup (WA97) in this conference, the observed m_T -spectra of hadrons from NA44 [20], NA49 [7, 21, 22], WA97 [23], and WA98 [24], in Pb+Pb collisions at $E_b =$

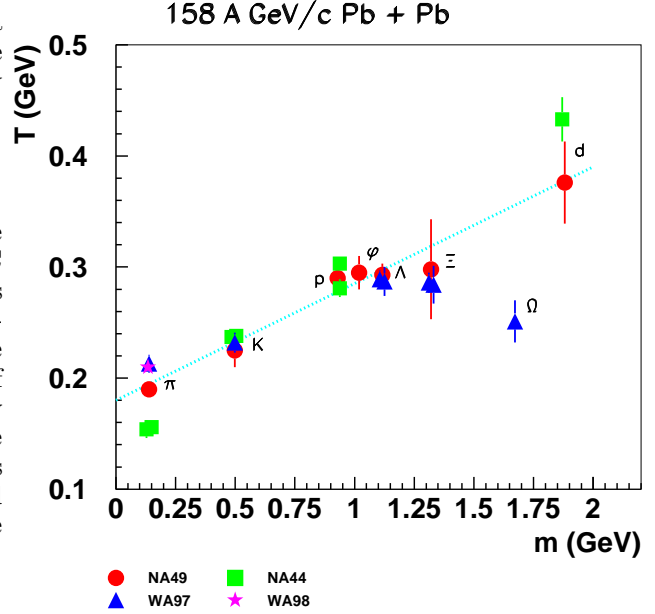


Figure 5. Mass dependence of the inverse slopes T_{slope} of the m_T -distributions. The fit is of the form $dN/dm_T^2 \sim \exp[-m_T/T_{slope}]$ as compiled in [18]. The data is from [7, 20, 21, 22, 23, 24] and the figure is from the SPS-summary [19].

158 AGeV, have been fitted to extract the inverse slope parameters T_{slope} as a function of the particle rest mass. Provided that the particles freeze out at approximately the same temperature, T_{slope} should clearly increase with mass. This indeed seems to be the case, as seen in the figure, with a notable exception of Ω , perhaps also that of Ξ . It has been suggested that due to their low interaction cross sections, these particles freeze out earlier and thereby benefit less of the transverse flow [25].

The average transverse momentum has also been observed to grow with the size, as shown in Fig. 6. Obviously, while the general features are consistent with a collective picture, some details i.e. behaviour of Ω (and Ξ), are not yet fully understood, and more work remains to be done on the theory.

2.2. Asymmetric flow

A feature in URHIC that in hadron-hadron collisions cannot in practice be addressed at all, are the non-central collisions, i.e. collisions with non-zero impact parameter b . For details of the asymmetric flow effects, I refer to a review [27], but to get some intuition, let us look at Fig. 7, which is a snapshot of an $A+A$ collision projected in the transverse (azimuthal) plane at the

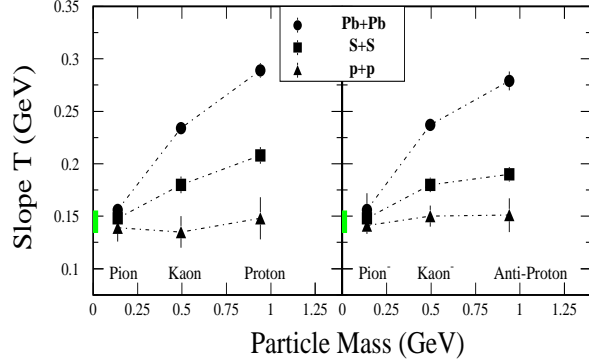


Figure 6. The dependence of the inverse slope parameter on the size of the system as function of mass as observed by the NA44 Collaboration. The figure is from [26].

time of maximum overlap of the colliding nuclei. The generated pressure gradients will obviously be azimuthally asymmetric when $b \neq 0$. Transverse flow is generated by the pressure gradients in the transverse plane, so it will evidently be azimuthally asymmetric: $\langle v_x \rangle \neq \langle v_y \rangle$. This in turn causes the azimuthal angle distributions of final state hadrons to be asymmetric.

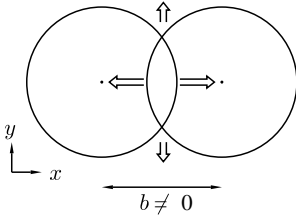


Figure 7. A non-central collision projected in the transverse-coordinate plane, illustrating the initial azimuthal asymmetry in the forming pressure gradients (the arrows).

To see the azimuthal asymmetry in the measured transverse momentum distributions, a Fourier analysis is performed, and a fit of the form

$$F(\phi) \sim 1 + 2v_1 \cos \phi + 2v_2 \cos 2\phi + \dots \quad (3)$$

can be used in each bin of rapidity. In practice, it suffices to consider the first two coefficients v_1 and v_2 . Figs. 8 illustrate the two types of asymmetry: purely directed flow with $v_1 \neq 0$ and $v_2 = 0$ and purely elliptic flow with $v_2 \neq 0$ and $v_1 = 0$. The measured angular distributions are then a mixture of these two effects.

With the high precision data coming from the SPS, it has indeed now become possible to observe the few percent asymmetries in the azimuthal angle distributions. NA49 collaboration has measured the

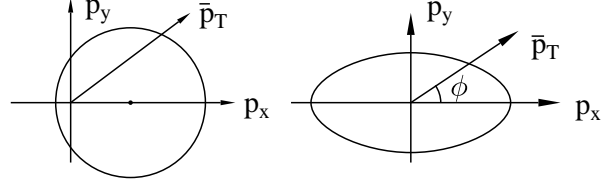


Figure 8. Purely directed (at left) and purely elliptic (at right) flow patterns as the azimuthal asymmetries of the transverse momentum distributions.

asymmetries in pion and proton distributions as functions of rapidity [28, 29]. As an example, the recent results from [29] for the Fourier coefficients v_1 and v_2 for the pion spectrum are shown in Fig. 9. For the results from NA52, see [30] and from WA98, see [31].

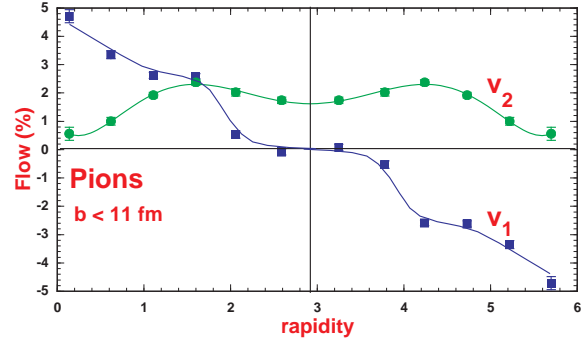


Figure 9. The observed azimuthal asymmetries in the transverse momentum distributions of pions in Pb+Pb collisions at $E_b = 158$ AGeV as function of rapidity and with impact parameters $b < 11$ fm, as measured and analysed by NA49 [29].

The existence of elliptic flow at the central rapidity (where the directed flow is zero) is a signature of pressure, and thereby collectivity, in the system. Once this signature is found, it is useful to scan the effect as a function of impact parameter, which controls the energy density reached. An abrupt behaviour as a function of b would be a direct signature of a QCD phase transition [32]. In the (preliminary) analysis [29] of the NA49 data no unexpected behaviour has been observed so far.

2.3. Particle ratios and thermal models

Above we saw how the experimental results support the existence of flow and collectivity in the system. The flow effects are expected to change the momentum distributions of final state hadrons but the total (full coverage 4π) yields of each hadron species should not, however, be sensitive to the

changes in the differential distributions. In fact, it can be shown that if all the fluid cells freeze out at the same temperature T_{fo} and at the same baryochemical potential μ_B^{fo} everywhere, the cancellation of flow effects in the particle ratios is complete. Under these conditions, the underlying dynamics of the system can be ignored, and purely thermal models can be used to predict the particle ratios. The results should then depend only on T_{fo} and μ_B^{fo} , and by fitting the measured (full coverage) particle ratios with the predictions of thermal models, T_{fo} and μ_B^{fo} can be extracted.

Quite obviously, however, the particle spectra cannot be measured with a 4π -coverage but some extrapolation is always needed to get the actual 4π -particle ratios. Secondly, the system is not likely to freeze out with the same T_{fo} and μ_B^{fo} everywhere, (in the forward and backward region the net baryon density is more than in the middle), so when discussing a thermal model fit to the data, one effectively considers a substitution of the local quantities $T_{fo}(x)$ and $\mu_B^{fo}(x)$ by global averages $\langle T_{fo} \rangle$ and $\langle \mu_B^{fo} \rangle$. The good news, however, is that the hydrodynamical simulations [33] show that only $\mathcal{O}(10 - 15\%)$ deviations from $\langle T_{fo} \rangle, \langle \mu_B^{fo} \rangle$ are expected at the SPS energies. This implies that thermal model approach is a reasonable first approximation for extracting the freeze-out parameters T_{fo} and μ_B^{fo} . For more discussion and references, see e.g. [2, 34].

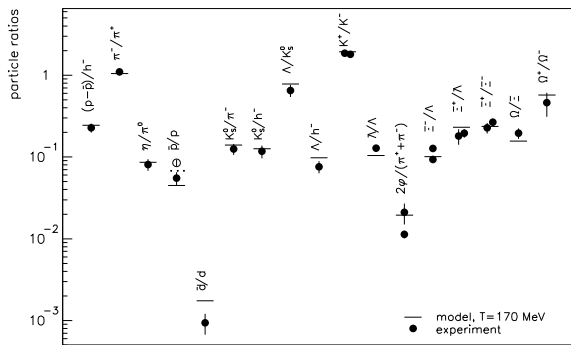


Figure 10. Particle ratios as obtained in a thermal model [35] with $T_{fo} = 170$ MeV and $\mu_B^{fo} = 270$ MeV as a best fit to the measured particle ratios from NA44, NA49, WA97, WA98 and NA50.

As an example of a recent thermal model analysis, the results for particle ratios from [35] are shown in Fig. 10. The analysis is straightforward: a grand-canonical ensemble is used to describe a thermal system of hadrons at a certain global

temperature T_{fo} , in a volume V and at (global) chemical potentials $\mu_B^{fo}, \mu_S, \mu_{I_3}$. Conservation of net baryon number, strangeness and charge, correspondingly, fixes V, μ_S and μ_{I_3} , leaving T_{fo} and μ_B^{fo} as the parameters which are fitted to an extensive collection of data. In addition, the hadronic interactions must be modelled into the partition function, and one should also allow for decays as well (see [35] for details). The best fit to the data from NA49 [7, 37, 22, 38, 21], NA44 [20], WA98 [39], WA97 [40, 41] and NA50 [42], gives $T_{fo} = 170$ MeV and $\mu_B^{fo} = 270$ MeV.

The results shown in Fig. 10 indicate that the measured particle ratios can indeed be quite well described by a system in thermal and chemical equilibrium. Thus a picture of a collective system in thermal and chemical equilibrium is emerging. The remaining differences between the model and the data are within the systematic uncertainties of the model and between different data sets [2]. I should also mention that there has been a lot of discussion whether the total strangeness is in chemical equilibrium or not [43]. In light of the analysis [35], additional fugacities are not necessary.

2.4. Identical particle interferometry

The main goal of identical particle interferometry, analogous to Hanbury Brown-Twiss (HBT) interferometry of stellar objects [44], is to extract a space-time picture of the system at freeze-out. By using the measured correlation functions in the momentum spectra of two (or more) identical pions, it is possible to estimate the emission volume (homogeneity volume), lifetime of the system and duration of the emission process (i.e. freeze-out). Also information on collectivity, i.e. transverse flow, is obtained. For more detailed reviews of HBT-theory and measurements in URHIC, I refer to [45, 46, 47, 48], here I will only describe the basic idea.

Let us imagine an emission of two pions with momenta p_1 and p_2 where the sources are a distance R apart. Relative momentum is denoted by Q , as in Fig.11, left panel, and the total momentum by K .

The two-particle correlation function is defined as

$$C_2(p_1, p_2) \sim \frac{dN/d^3p_1 d^3p_2}{dN/d^3p_1 dN/d^3p_2} \quad (4)$$

and it can be directly measured. The one-particle distributions (which are measured) are expressed in terms of space-time integrals of source functions $S(x, p)$: $dN/d^3p_1 = \int d^4x S(x, p)$. The source functions contain all the information of the system

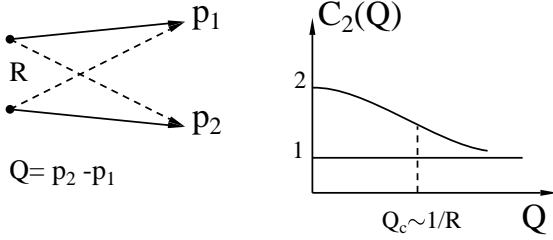


Figure 11. Left: Emission of two pions from two sources separated by R (a coordinate 4-vector). Right: The width of the corresponding (measured) two-pion correlation function $C_2(Q)$ reflects R : $Q_c \sim 1/R$.

at freeze-out, including the transverse flow. The non-trivial task is to unfold this information by using the measured correlation functions.

The two-boson correlation function can be written in terms of the source functions as [49]

$$C_2(Q, K) = 1 + \frac{|\int d^4x e^{iQ \cdot x} S(x, K)|^2}{\int d^4x S(x, p_1) \int d^4y S(y, p_2)}. \quad (5)$$

The quantitative details naturally depend somewhat on the physical assumptions made for the functional form of the source function but the basic idea remains the same: the source radius can be determined from the width Q_c of the measured correlation function, $Q_c \sim 1/R$, as illustrated in Fig. 11.

In particular, it should be noted that unlike emission from the stars, which are static objects, emission from URHIC is a dynamic process. Consequently in HBT for URHIC, the spatial and temporal dimensions are non-trivially mixed, and several different radius parameters have to be defined. Usually K is chosen to be in the x, z plane with the beam in z -direction. Then the radius parameters are R_L , R_{out} and R_{side} in the z -, x - and y -direction, correspondingly.

As an example of an HBT-measurement, let me show the one by NA44 in Fig. 12 [50]. The remarkable physics point here is that a typical scale $\mathcal{O}(20 \text{ MeV}) \sim \mathcal{O}(10 \text{ fm})$ is clearly seen in the high precision data of two-particle correlation functions. For the most recent experimental HBT analyses, see the results from NA44 [52], NA49 [51], WA98 [53], and the talk by Ganz (NA49) in this conference.

As reviewed in [47], when space-time information from HBT and complementary information from the m_T -distributions are combined, the freeze-out temperature of the system produced in Pb+Pb collisions is found to lie in the range $80 \text{ MeV} < T_{fo} < 120 \text{ MeV}$, a strong transverse flow is seen to develop, $0.35 < v_T < 0.5$, together with a large transverse extension $R_{fo} \sim 2R_{Pb}$, and lifetime

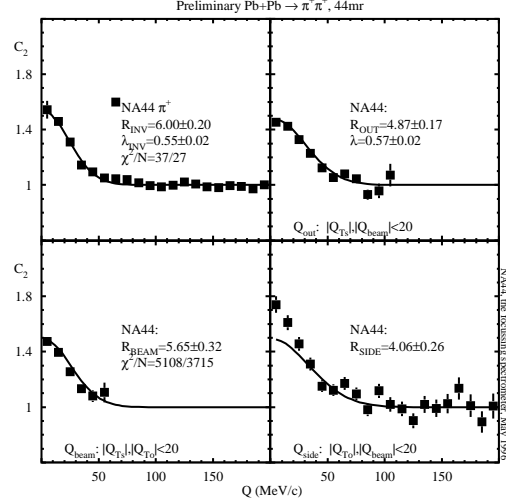


Figure 12. An example of the measured identical two-particle correlation functions in pion momentum distributions, measured by NA44 [50] in Pb+Pb collisions.

$\sim 10 \text{ fm}/c$. In comparison with the thermal model results in the previous section, a clear hierarchy is observed: *thermal* freeze-out observed in the HBT and in the transverse momentum distributions takes place later, i.e. at lower T , than *chemical* freeze-out which is in turn reflected by the hadron abundancies. This is consistent with the expectation that the chemical reaction rates are much smaller than the elastic ones.

2.5. Event-by-Event analysis

Large multiplicities in single central events allow the study of fluctuations of different observables on an event-by-event (EbyE) basis. Also this is a feature of URHIC genuinely different from hadron-hadron collisions. Naturally, the primary goal of the EbyE physics is to observe differences between the events with and without QGP-formation, as the QCD phase transition may cause large fluctuations which could show up in measurable quantities like multiplicities, $\langle p_T \rangle$, particle ratios, etc in single events. Especially, if the QCD phase transition is of second order, one might directly observe the critical fluctuations associated with the phase transition. Also, if some more exotic physics takes place, such as formation of large enough domains of disoriented chiral condensates (DCC) [54], the fluctuations from one event with DCC to another without could be seen.

Fig. 13 shows the recent EbyE results from NA49 [55]. So far no evidence of non-trivial dynamical fluctuations, i.e. fluctuations beyond

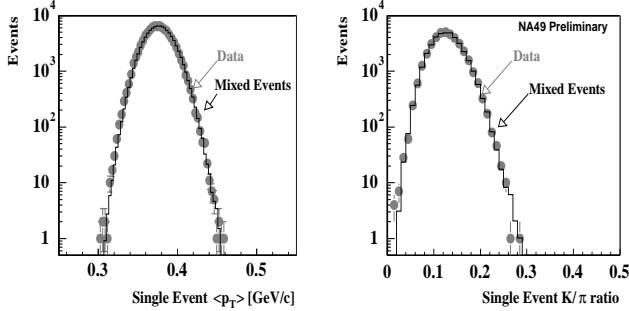


Figure 13. Event-by-event fluctuations of single event $\langle p_T \rangle$ (left) and single event K/ π -ratio (right), measured by NA49 in Pb+Pb collisions at the SPS. The dynamical event-by-event fluctuations are $< 1\%$ in $\langle p_T \rangle$ and $< 4.9\%$ in K/ π . The figure is from [55].

finite statistics and variations of impact parameter, has been observed in the Pb+Pb collisions at SPS: the dynamical event-by-event fluctuations are less than 1% in single event $\langle p_T \rangle$ and less than 4.9% in K/ π -ratio (at 90 % confidence level). It will indeed be very interesting to see what the corresponding results will be in URHIC at RHIC and LHC/ALICE.

2.6. Strangeness enhancement

The observables discussed in the previous subsections support the interpretation of the the system produced in Pb+Pb collisions at the SPS as a collective strongly interacting system. Let me now move on to other experimental facts, namely the observed anomalies. First, let us have a look at the strangeness enhancements observed. For more detailed reviews and for more complete list of references to the measurements of strangeness production in URHIC, see e.g. [56,57].

In comparison to hadron-hadron and e^+e^- collisions, a *global enhancement* of strangeness production has been observed in URHIC. At the SPS, the first observation of this was made by NA35 [58] in S+S collisions at $E_b = 200$ AGeV. The global enhancement can be quantified by defining a parameter which counts the strange quark-antiquark pairs produced relative to the $u\bar{u}d\bar{d}$ produced [59]

$$\lambda_s^{AA} \equiv \frac{2\langle s + \bar{s} \rangle}{\langle u + \bar{u} \rangle + \langle d + \bar{d} \rangle} \approx 2\lambda_s^{pp} \quad (6)$$

This indicator is plotted in Fig. 14 for S+S and S+Ag at $E_b = 200$ AGeV based on the data from NA35 [60], and for Pb+Pb collisions at

$E_b = 158$ AGeV based on the measurements by NA49 [36,61] and compared with the corresponding compilation of data from e^+e^- , p+p and p+ \bar{p} collisions (for the refs, see [59]). The observation is that $\lambda_s^{AA} \approx 2\lambda_s^{pp,ee}$: the global strangeness enhancement is thus a unique feature of URHIC.

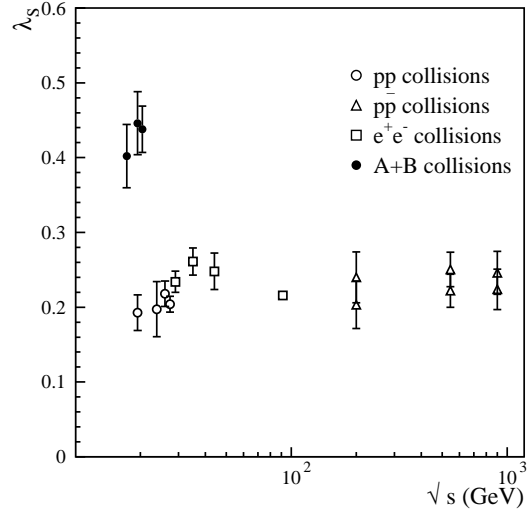


Figure 14. The global strangeness is observed to be enhanced by a factor ~ 2 in A+B (S+S, S+Ag and Pb+Pb) relative to e^+e^- , p+p and p+ \bar{p} collisions. The figure is from [59].

In addition to the global enhancement, also *specific enhancements* in the production of $K, \bar{K}, \Lambda, \bar{\Lambda}, \Xi, \bar{\Xi}, \Omega, \bar{\Omega}$ and ϕ at midrapidity in Pb+Pb collisions relative to that in p+Be collisions have been reported by the WA97 [62,63], NA49 [55,64] and NA50 [65] collaborations. The multi-strange hadron yields, in particular, are strongly enhanced in central Pb+Pb collisions, as seen in Fig. 15, where the yields per participants relative to pBe, measured by WA97, are plotted as a function of the average number of participants in p+Pb and Pb+Pb collisions at the SPS [62]. For more details, see the talk by Helstrup (WA97) in this conference.

Notice especially that the number of negative hadrons scales with the number of participants, and relative to the charged hadrons the enhancement in $\Omega^- + \Omega^+$ yield is roughly a constant factor 10. With the 1998 run, the Pb+Pb event statistics was practically doubled, and WA97 will soon cover the region below 100 participants (see Helstrup and [62]). It will certainly be very exciting to see whether there is a threshold in the number of participants (centrality) after which the strong specific strangeness enhancement takes place.

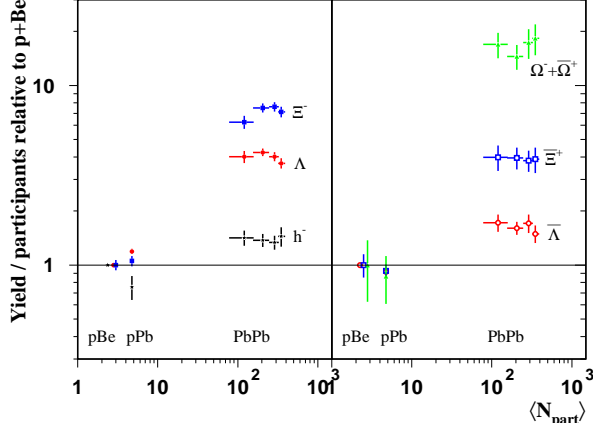


Figure 15. The specific strangeness enhancement as measured by WA97. The yields per participant per unit rapidity relative to p+Be as a function of the number of participants (centrality) [62].

What are the implications of these experimentally observed facts? If the produced dense system consists of *uncorrelated* quarks (and antiquarks), it is intuitively clear that the more a hadron contains strange quarks (or antiquarks) the more it benefits of the global strangeness enhancement in hadronization. This picture is quantified in statistical hadronization (quark coalescence) models [66], which seem to work for $A+A$ collisions but not for $p+A$ collisions. On the other hand, hadronic kinetic models do not reproduce the data on multi-strange hadrons due to high mass-thresholds and low chemical reaction cross sections. Also approaches with string breaking followed by hadron rescattering models (see [62] for the actual comparison and for further references) cannot reproduce the centrality pattern observed. The implication of the observed strangeness enhancement therefore is that the quark degrees of freedom are indeed essential, and that strangeness must have been produced very early on in the collision, in the pre-hadronic stage.

From the thermal models (Fig. 10), we remember that the particle ratios, including those with multi-strange hyperons are close to chemical equilibrium values. This, together with the conclusion of the importance of the quark degrees of freedom, points towards thermalized QGP.

2.7. Low-mass e^+e^- enhancement

Another very interesting anomaly observed in URHIC at the SPS is the excess of electron-positron pairs in the mass region

$250 \text{ MeV} \lesssim M_{e^+e^-} \lesssim 700 \text{ MeV}$, usually referred to as the “low-mass” region. The excess in e^+e^- production was first observed by NA45/CERES in S+Au collisions at $E_b = 200 \text{ AGeV}$ [67, 68, 71], and a similar excess was observed in $\mu^+\mu^-$ by the HELIOS-3 collaboration in S+W collisions at $E_b = 200 \text{ AGeV}$ [69], and by NA38 [70] in S+U at $E_b = 200 \text{ AGeV}$. The low-mass excess has been confirmed by CERES for heavier systems in Pb+Au collisions at $E_b = 158 \text{ AGeV}$ [72, 73].

The reference data is given by the e^+e^- production in p+Be and p+Au collisions at $E_p = 450 \text{ GeV}$: no enhancement is observed there, the data can be explained by including contributions from all the known hadron decays. The mass distributions of e^+e^- -pairs measured in p+Au by CERES [74] and scaled by the measured charged particle multiplicity (within the CERES acceptance) are shown in Fig. 16. The cocktail of the several different sources of e^+e^- -pairs is shown, and it is seen to reproduce the measured data within the estimated errors (the shaded band) quite well.

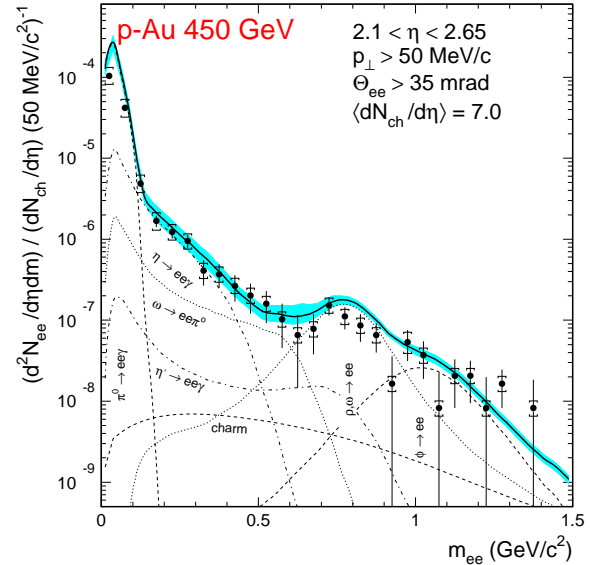


Figure 16. Inclusive mass distribution of e^+e^- -pairs in p+Au collisions at 450 GeV scaled with charged particle multiplicity [74]. The curves are the known sources from hadron decays.

However, when one extrapolates the cocktail-plot to S+Au and Pb+Au collisions, a clear enhancement is observed, as shown in Fig. 17 [73] for the mass distributions of e^+e^- -pairs scaled by the charged particle multiplicity. In the figure, data sets from ’95 and ’96 are compared with the sum

of the expected contributions from hadron decays. In the cocktail-plot the particle ratios are taken from a thermal model fitted to measured ratios in Pb+Pb ($T_{fo} = 175$ MeV and $\mu_B = 270$ MeV, fig.10), and the η - and p_T -distributions follow the measured systematics in Pb+Pb collisions. The enhancement in the mass-region $250 \text{ MeV} \lesssim M_{e^+e^-} \lesssim 700 \text{ MeV}$ is observed to be $2.6 \pm 0.5(\text{stat}) \pm 0.6(\text{syst})$ for the '96 data set, and $3.9 \pm 0.9(\text{stat}) \pm 0.9(\text{syst})$ for the '95 data set [73]. The excess has been observed to concentrate at low pair transverse momentum.

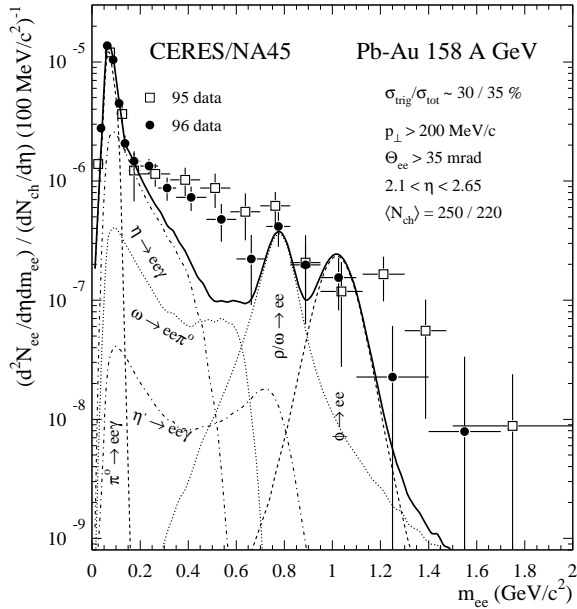


Figure 17. Low-mass enhancement of e^+e^- -pairs in Pb+Au collisions at $E_b = 158$ AGeV [73].

Interestingly, the excess scales more strongly than linearly with charged particle multiplicity, suggesting that it is due to a medium-effect. The shape of the mass-spectrum is not consistent with $\pi^+\pi^-$ annihilation in free space, either, which again supports a medium-effect as the origin of the low-mass enhancement. There has been considerable theoretical activity in trying to explain the effect. For recent reviews, see [14, 75, 72]. The suggestions vary from a collisional broadening of the ρ -meson (i.e. ρ has a shorter lifetime in a dense hadronic medium, which leads to a broader peak in the mass distribution) and in-medium modifications of the ρ spectral function [14, 75] to a possible change in the mass of ρ [76].

Let me also show the dielectron results from [77] based on a hydrodynamical simulation where the whole space-time evolution of the system is taken

into account [78]. In this approach, the total yield of dielectrons (and dileptons in general) consists of the pairs from the decays of resonances originating from the freeze-out surface (see Fig. 3), and of the thermal dielectrons emitted from the dynamically evolving fireball throughout its whole space-time evolution. The measured hadronic momentum spectra are first reproduced to constrain the hot initial state and the EoS simultaneously [78]. After this, the emission of thermal e^+e^- -pairs can be predicted by using the thermal rates [79, 75] at each local T and μ_B . The e^+e^- contribution from the resonance decays alone is shown in Fig. 18 by the upper panel. Adding the thermal pairs gives the lower panel. We observe that that thermal emission dominates the total yield of e^+e^- -pairs in the region of the experimentally observed excess. Let me also remind that the low-mass enhancement is *not* considered to be a direct signal of QGP: contribution of thermal emission from the QGP-phase is negligible in the region of the low-mass enhancement (see [77]).

Although theoretically still not fully resolved, it is evident that with the low-mass enhancement of e^+e^- -pairs measured by CERES, we are having a first glimpse into the dynamics of mesons in baryon-rich environment exceeding a temperature $T \sim 120$ MeV. In the near future, CERES will collect more data, also with the lower energy beams ($E_b = 40$ AGeV) and include an additional TPC in the experimental setup [73]. With improved statistics, and a better mass-resolution and signal-to-background ratio, CERES will certainly shed more light to the details of low-mass dielectron excess as a signature of a hot hadronic gas.

Regarding the observed dilepton mass spectrum in general, let me note that also the intermediate mass dimuons, $1.5 \text{ GeV} < M_{\mu\mu} < 2.5 \text{ GeV}$, show an excess relative to the conventionally known sources, as observed by NA38 in S+U [80], and HELIOS-3 in S+W collisions at $E_b = 200$ AGeV [69], and NA50 in Pb+Pb at $E_b = 158$ AGeV [81]. It will be interesting to see whether this excess could also be explained by production of thermal dileptons [82].

2.8. J/Ψ suppression

Of the anomalies observed in URHIC at the SPS, the one that has generated most excitement, is the anomalous suppression of J/Ψ in central Pb+Pb collisions at $E_b = 158$ AGeV, observed by the NA50 collaboration [83, 84, 85, 86, 87]. The idea of studying the suppression of J/Ψ production as a signal of the QGP originates from Satz and Matsui in 1984 [88]: formation of J/Ψ bound state should be very efficiently Debye screened in QGP. For

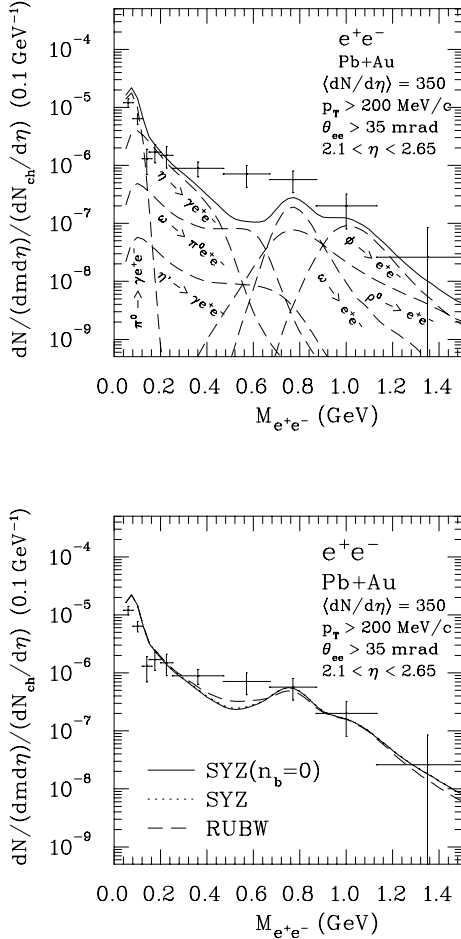


Figure 18. Mass spectrum of e^+e^- -pairs scaled with charged particle multiplicity as predicted by a hydrodynamic simulation [77]. Upper panel: contribution from the hadron decays. Lower panel: total yield, which includes the thermal emission.

details of the NA50 measurements and analysis, see [87] and the talk by De Falco (NA50) in this conference. For a more detailed overview of the theory of J/Ψ suppression, see e.g. [89, 90, 91] and the talk by Nardi in this conference.

The key question naturally is relative to what the J/Ψ suppression appears in the heaviest URHIC systems. As shown in Fig. 19 [84], a clear and smooth suppression pattern is observed from p+p and p+d collisions to p+A and S+U collisions, as measured by the NA38 and NA51 collaborations [92]: $B_{\mu\mu}\sigma(J/\Psi)$ is decreasing as a function of $A*B$. For the comparison, the measurements have been rescaled to the same \sqrt{s} . A scaling $B_{\mu\mu}\sigma(J/\Psi) \sim (AB)^{0.92}$ is found [84]. As seen in the figure, the J/Ψ in Pb+Pb collisions clearly deviate from

the pattern of normal nuclear suppression. The additional suppression of J/Ψ in Pb+Pb collisions is often referred to as the “anomalous” one.

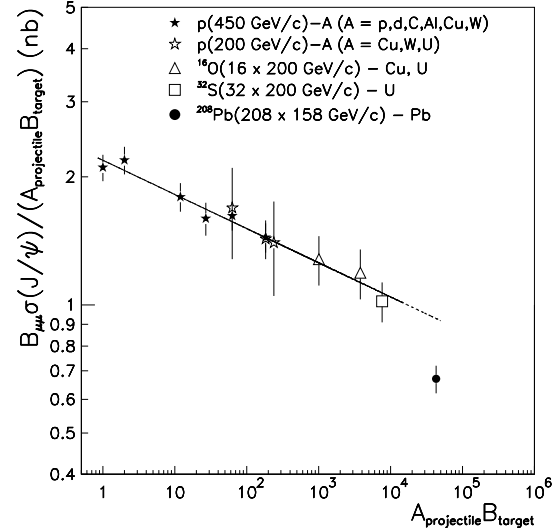


Figure 19. Suppression of J/Ψ production as a function of AB : normal nuclear suppression from p+p to p+A and to S+U, and anomalous suppression in Pb+Pb. The figure is from NA50, ref. [84].

At the same time, the Drell-Yan (DY) dilepton production at is *not* observed to be suppressed [84]†: $\sigma(DY)_{\text{exp}}/\sigma(DY)_{\text{th}} \sim AB$. Obviously then the suppression of J/Ψ comes from the final state interactions, i.e. from absorption of the produced bound state within normal nuclear matter (the beam and target). The nuclear absorption, often called as “normal” suppression, can be understood in Glauber-type models, see [94, 96] for details. For discussion of the absorption by hadronic comovers, see [95]. The observed nuclear absorption pattern (Fig. 19) can be reproduced by using absorption cross-sections of the J/Ψ (or its pre-hadronic state) of the order of 6...7 mb [84, 96]

NA50 has also carefully studied the suppression as function of transverse energy E_T . In each Pb+Pb collision, the produced transverse energy and the energy observed in the zero-degree calorimeter correspond to an impact parameter b . The produced $c\bar{c}$ -pair bound state which is to form a J/Ψ first has to go through the rest of the projectile and the target, so for each b (E_T) there is an average

† The Drell-Yan computation here assumes that any nuclear effects in the parton distributions [93] are negligible within the errorbars.

nuclear path length L which the pre-resonance has to survive. The measured Drell-Yan pairs serve as a non-suppressed background in each E_T -bin, i.e. at each b , and $B_{\mu\mu}\sigma(J/\Psi)/\sigma(DY)$ can be plotted both as a function of E_T and as a function of L , as shown in Figs. 20, 21 and 22 [86]. The DY cross section $\sigma(DY)$, against which $B_{\mu\mu}\sigma(J/\Psi)$ is compared, is computed at $2.9 \text{ GeV} < M < 4.5 \text{ GeV}$ by using the measured DY-pairs at $M > 4.5 \text{ GeV}$ to get the correct normalization (Note that equally well one could directly use the measured Drell-Yan pairs; this has also been done by NA50 but is not shown here).

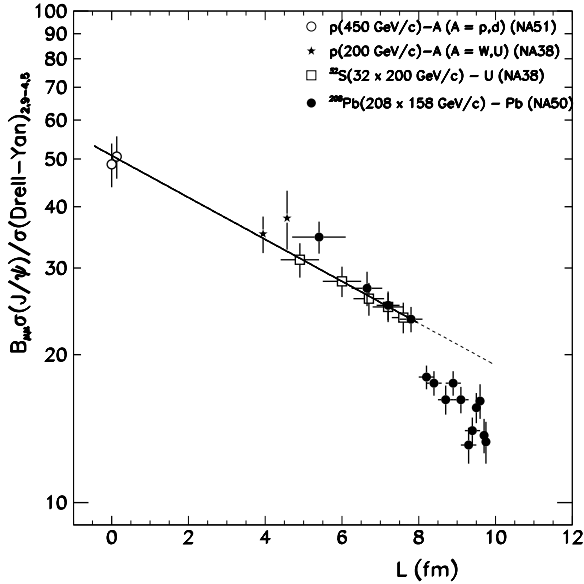


Figure 20. The suppression of J/Ψ over Drell-Yan pairs in $2.9 \text{ GeV} < M < 4.5 \text{ GeV}$ as a function of the average nuclear path length L of the $c\bar{c}$ pre-resonance [86], for NA38, NA50 and NA51 data. The NA50 Pb+Pb data (filled circles) is from the 1996 run.

In Fig. 20, the filled circles at largest values of L represent the most central Pb+Pb collisions, and the ones at smallest L correspond to impact parameters $\langle b \rangle = 10.8 \text{ fm}$ [86]. The peripheral Pb+Pb are seen to coincide with lighter systems, as one would expect to. It is also interesting to divide out the normal nuclear suppression and replot the suppression, as done in [86], from where I have borrowed also Fig. 21. Notice here the importance of the p+p and p+d points (*not* shown in this figure) in determining the amount of normal nuclear suppression of J/Ψ at large values of L . The filled circles show the results from the new minimum bias

analysis of NA50 [86], as discussed by De Falco at this conference. The abrupt drop seen in the figure for the J/Ψ suppression in Pb+Pb is the best candidate so far for a threshold behaviour in URHIC at the SPS. Naturally, the hope is that this would be the first direct observation of the QGP formation in the central Pb+Pb collisions.

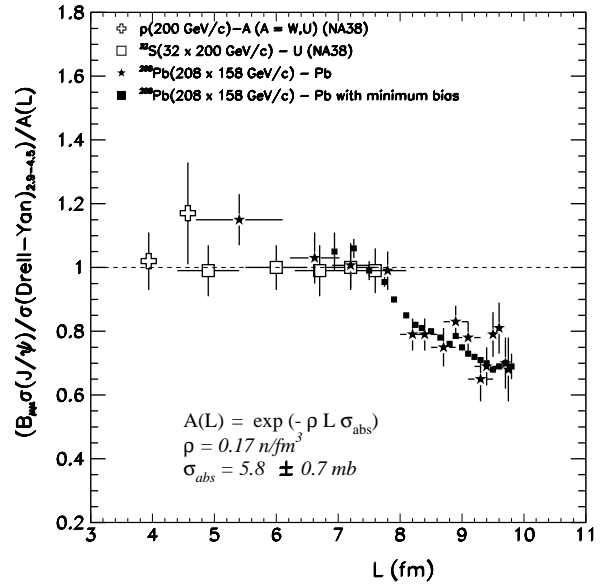


Figure 21. The same as in the previous figure but the with the normal nuclear suppression divided out [86]. The Pb+Pb data is from 1996 run, and also the new minimum bias analysis is shown (the filled squares). In comparison with the previous figure, notice here the different scale in L .

Fig. 22 from [86] shows the suppression of J/Ψ over Drell-Yan directly as a function of the measured E_T , as obtained in the two different analyses of the data from 1996 run. The 15 E_T bins correspond to the 15 bins in L in the previous figures and the solid line represents the expectation for the normal nuclear suppression as shown in the previous figures. Here, one should again keep in mind the importance of the lighter systems in determining the solid line. The suppression pattern is, naturally, the same as in the previous figures.

Interestingly, as recently reported by NA50 [87], there may actually be *another drop* in the J/Ψ suppression pattern at the largest values of E_T . The latest (preliminary) analysis of the 1998 data is shown in Fig. 23 from ref. [87]. As discussed in [87], the second drop was not observed in the data from 1996 run, where a thicker target was used, because

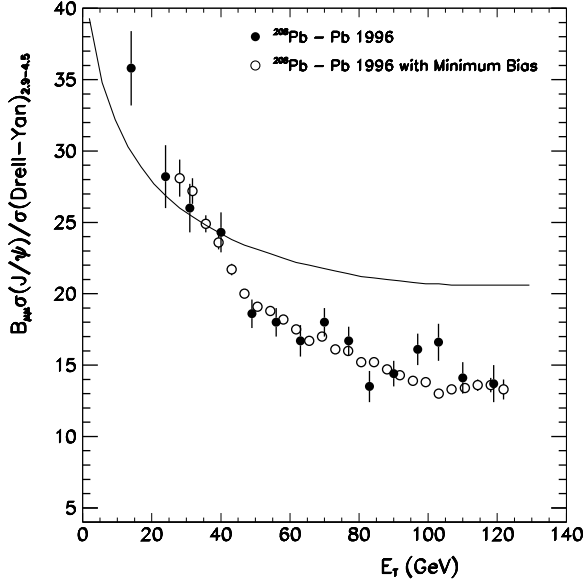


Figure 22. The ratio $\sigma_{J/\Psi}/\sigma_{DY}$ at $2.9 \text{ GeV} < M < 4.5 \text{ GeV}$ in Pb+Pb collisions as a function of E_T [86]. The 1996 data is analysed in two different ways, see [86] for details.

of a bias from re-interaction events. This problem is removed in the 1998 set up. The possibility for a second drop is indeed very exciting, and it would support the prediction in [97] of melting of different $c\bar{c}$ bound states at different energy densities.

For a future improvement, the possibility to add a new vertex detector into the NA50 setup is discussed. This suggestion, called NA6i, was also presented in this meeting by Shahoyan. The benefit of this would be that open charm contribution could be measured more accurately, and this would serve as a very useful background both for the J/Ψ suppression measurements and for the intermediate mass muon pairs.

For a compact review of the theoretical interpretations of the observed J/Ψ suppression, let me suggest [89], see also the talk by Nardi in this conference. As one is discussing formation and interactions of a QCD bound state, perturbative calculations are hard to do. Consequently, different models have been presented, see e.g. [94, 95, 98, 96, 99, 100, 101, 90, 91]. Several questions, like the energy dependence of the dissociation cross section of the $c\bar{c}$ -pair [102, 103], and applicability of QCD factorization in the bulk production of J/Ψ in AA-collisions have been and are still discussed. Even if all the details are theoretically not yet fully known, there seems to be a general consensus on that while the normal nuclear suppression of

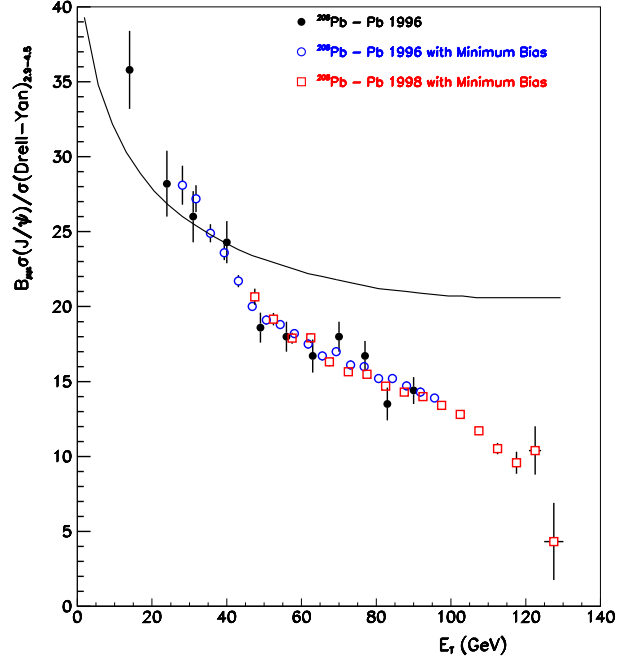


Figure 23. Preliminary analysis of the 1998 data for suppression of J/Ψ and comparison with the analyses of the 1996 data. The figure is from [87].

J/Ψ can be accounted for by a more conventional hadronic picture, to reproduce the anomalous suppression, especially with the observed abrupt behaviour - possibly even with two drops - an additional ingredient very efficient in destroying the $c\bar{c}$ bound state is needed. Putting this together with the implications of a collective system and of the importance of partonic degrees of freedom, as discussed in the previous sections, it is very likely that we are now finally looking at a deconfined phase of QCD-matter.

3. The future: RHIC & LHC/ALICE

3.1. RHIC: Relativistic Heavy Ion Collider

Until now the fixed target experiments at the SPS at $\sqrt{s} \sim 20 \text{ AGeV}$ have been the URHIC of highest collision energy. The next step will be taken by the Relativistic Heavy Ion Collider (RHIC) at Brookhaven National Laboratory, where ^{197}Au -beams will be collided onto ^{197}Au -beams at $\sqrt{s} = 200 \text{ AGeV}$, and luminosity $L \sim 10^{26..27} \text{ cm}^{-2}\text{s}^{-1}$. RHIC will also collide proton-beams with proton-beams at $\sqrt{s} = 500 \text{ GeV}$ and $L = 10^{31} \text{ cm}^{-2}\text{s}^{-1}$, and make p+A and A+B collisions with various A and B. Collisions with polarized protons will also be done. At the time of the this meeting, beam tests

were being done in the two rings, with the aim to get the collider in operation in December 1999§ [104].

Without going to any details, let me here just list the heavy-ion experiments at RHIC, together with their main physics goals. For a more complete review, see e.g. [105]. The main goal of RHIC will be to study the strongly interacting matter produced at URHIC, and to observe the QGP through various independent signals. Thanks to the varying beams and cms-energies, RHIC will provide us with an extensive \sqrt{s} - and AB -systematics, which will be important in comparing the events with and without QGP formation.

There are four major heavy-ion experiments at RHIC, involving O(900) scientists and O(80) institutions. There are two “large” experiments, STAR (Solenoidal Tracker at RHIC) [106] and PHENIX (Pioneering High Energy Nuclear Interaction Experiment) [107], and two “small” ones, BRAHMS (Broad Range Hadron Magnetic Spectrometer) [108] and PHOBOS [109].

The main elements of the STAR experiment are silicon vertex tracker system (SVT), time projection chamber (TPC), forward radial-drift TPC (FTPC), time of flight measurement system (TOF) and electromagnetic calorimeter (EMC). The primary physics goal of STAR is to study strongly interacting matter at high densities in central $A+B$ collisions. This will be achieved by measuring hadrons over a large solid angle, and measuring the global observables on an event-by-event basis. STAR will also study peripheral $A+B$ collisions and polarized p+p collisions.

The main building blocks of the PHENIX experiment are multiplicity vertex detector (MVD), ring-image Cherenkov counter (RICH), time-expansion chamber (TEC), TOF and EMC. PHENIX will mainly concentrate on measuring leptons, photons and hadrons to search for the QGP signatures.

BRAHMS is a forward and mid-rapidity hadron spectrometer. The physics goal is to make a systematic study of particle production in AA collisions from the peripheral to the most central impact parameters. BRAHMS should basically answer the question of where the baryons go. PHOBOS is a compact multiparticle spectrometer which will measure single particle spectra and correlations between particles with low transverse momenta and to characterize events using a multiplicity detector.

3.2. ALICE: A Large Ion Collider Experiment

The ultimate step in the cms-energy of URHIC will be taken by A Large Ion Collider Experiment, ALICE [110] at the Large Hadron Collider (LHC) at CERN in 2005. ALICE will be the only detector at the LHC dedicated for URHIC.

The heaviest beams colliding at ALICE will be $^{208}\text{Pb}+^{208}\text{Pb}$ at $\sqrt{s} = 5.5 \text{ ATeV}$. The luminosity in these collisions, $L = 2 \cdot 10^{27} \text{ cm}^{-2} \text{ s}^{-1}$, corresponds to some 10^4 interactions/s. ALICE will also perform p+p and p+A collisions to collect reference data for Pb+Pb, and it will also make $A+B$ and $A+A$ collisions with lighter nuclei to vary the produced densities of the QGP. According to the present running scenario, the running time for heavy ions will be about 10% of the LHC year.

In comparison with SPS and RHIC, there are definite physics advantages in increasing the cms-energy as much as possible:

- net baryon density near $y \sim 0$ is smaller; $\mu_B \ll T$, and the EoS approaches that of the theoretically better understood $\mu_B = 0$ case
- initial QGP energy density is higher
- lifetime of the QGP phase and of the whole system is longer
- freeze-out volume is larger (in a comoving sense, the system never decouples simultaneously everywhere)
- one moves into the applicability region of perturbative QCD (pQCD): First, there will in general be higher rates for harder QCD-probes of the QGP, such as high- p_T jets, direct photons at high p_T , large mass dileptons, and upsilon production, and, second, the initial energy densities can be more reliably estimated based on perturbatively calculable quark and gluon E_T -production [111,112], see also the talk by Hammon at this conference, and, the approach of refs. [114]. Let me point out that the pQCD calculation has now been done consistently in next-to-leading-order pQCD [113].

In this conference, the detector overview and physics capabilities of ALICE were reviewed by Morsch (ALICE). The main goal of ALICE is to study the behaviour of strongly interacting matter through observing various independent QGP-signatures simultaneously. A recent review of the physics at ALICE can be found in e.g. [115]. Let me, however, list some examples below:

- The global observables, such as charged particle multiplicity at central rapidities, dN_{ch}/dy , and global transverse energy distributions

§ Some delays can now be foreseen.

dE_T/dy ($d\sigma/dE_T$) will be affected by the initially produced densities (initial transverse energy is not an observable unlike the final E_T) and subsequent pdV work done by the collective QGP-HG system against expansion [112].

- Event-by-event fluctuations will be measured in many observables, such as forward-energy, charge particle multiplicity, HBT-correlations, single event $\langle p_T \rangle$, particle ratios, N_{ch}/N_γ . In this way ALICE is expected to find the possible exotic events.
- The transverse momentum spectra and particle abundancies will be measured for all possible particle species ($\pi, \eta, \omega, \phi, p, K, \Lambda, \Xi, \Omega, D, d, t, \alpha, \dots$). These will reflect the flow effects and the freeze-out as discussed previously.
- Identical particle HBT-correlations will be measured to give information of the dynamical evolution, size and lifetime and phase-time structure of the freeze-out process.
- Open charm and open beauty measurements will provide a normalization for J/Ψ - and Υ -suppression. As hard probes, $c\bar{c}$ and $b\bar{b}$ are produced very early on in the AA collision. Consequently, they will be very sensitive to the early and hot QCD phase of matter.
- Energy-loss of high- p_T partons in QGP [116] can be studied via jet (and leading particle) measurements at ALICE. In this conference, the recent results on finite systems were discussed by Levai [117].
- Muons at $2 < \eta_\mu < 4$ will be measured and $\mu^+\mu^-$ will be studied. Especially interesting will be the dimuons coming from the decays of J/Ψ and Υ (if there are any $J/\Psi, \Upsilon$ to decay!), as these will be directly probing the deconfinement. Also intermediate mass muons will be very interesting, due to the contributions from several sources, such as the Drell-Yan process, decays of D - and B -mesons and thermal emission [119]. If e^+e^- pairs will also be identified, as lately suggested, modifications of the ρ, ω, ϕ -meson properties related to the low-mass behaviour of e^+e^- can be studied in detail.
- Hard photons will also be an important tool to study the QGP. Especially, in order to see any window for thermally radiated photons, the background of direct photons and decay photons needs to be fully understood. As discussed for RHIC [118], the direct photon-jet events can possibly also be used to study energy loss of partons in QGP. In these calculations, and in calculations of any hard probes of QGP, information of nuclear parton

distributions and their scale evolution [93] are needed. The data from p+A collisions will also be used to constrain the nuclear parton distributions.

To compare some global characteristics of URHIC at SPS, RHIC and LHC/ALICE, I have prepared the table 1. I would especially like to draw your attention to the expected long lifetime of the *QGP-phase* at the LHC which is of the same order of magnitude as that of the *whole* system at the SPS. Also, even though the system will not freeze out simultaneously everywhere in space (roughly simultaneous decoupling may happen in the transverse direction, except for the very edges, but longitudinally there will be strong time dilation effects at the LHC), I have defined a comoving volume by counting roughly how many units of space-time rapidity are available along a proper time curve. Notice how dramatic the increase in the “size” is when going from the SPS to the LHC: the rest frame volume of a lead nucleus is $V_{Pb} = 1150 \text{ fm}^3$, so $400V_{Pb} \sim 5 \cdot 10^5 \text{ fm}^3$, and compared with the nuclear size parameters, one is talking about almost “macroscopic” quantities of strongly interacting matter at the LHC!

To conclude the LHC-section for URHIC, let me also mention that the possibility of measuring J/Ψ , Υ and Z_0 production in Pb+Pb collisions in the CMS detector at the LHC is being discussed, see e.g. [115].

4. My conclusions

4.1. SPS

Analyses of several different observables from independent measurements at the SPS have shown that a picture of production of collectively behaving strongly interacting matter with large volume and finite lifetime is now finally emerging. The systems produced in collisions of heaviest nuclei (Pb+Pb, Pb+Au) are clearly different from the ones produced in nucleon-nucleon and proton-nucleus collisions.

Evidence of collective behaviour of matter is obtained from the measured hadron yields and momentum spectra (NA44, NA49, WA97, WA98, NA50, NA52): the systematic broadening of transverse momentum spectra (sec. 2.1) is compatible with a behaviour typical for a system with pressure and transverse flow. The observation of elliptic and directed flow (sec. 2.2) also strongly points to this direction (NA49, WA98, NA52). The thermal model picture of the system reproduces the measured particle ratios surprisingly well (sec. 2.3), and, the HBT analysis of correlations in

	SPS	RHIC	LHC
\sqrt{s}/A (GeV)	17	200	5500
ΔY	6	11	17
dN_{ch}/dy	400	700-1500	3000-8000
τ_{tr}^{PbPb} (fm/c)	1	0.1	0.005
τ_0^{QGP} (fm/c)	1	~ 0.2	0.1
$\varepsilon(\tau_0)$ (GeV/fm ³)	3	60	1000
τ_{QGP} (fm/c)	$\lesssim 2$	2-4	$\gtrsim 10$
τ_{fo} (fm/c)	~ 10	20-30	30-40
$V_{com}(\tau_{fr})$	$8V_{Pb}$	$90V_{Pb}$	$400V_{Pb}$

Table 1. Some characteristics of the heaviest systems produced in AA at SPS, RHIC and LHC ($A \sim 200$). From the top: cms-energy \sqrt{s} , available total rapidity interval ΔY , charged particle multiplicity dN_{ch}/dy at $y = 0$, the transit time τ_{tr} of the Lorentz-contracted nuclei, the formation time τ_0^{QGP} of the QGP (lower limit) [112], the initial energy density $\varepsilon(\tau_0)$ at the time of formation of the QGP [11, 112], lifetime of the QGP phase τ_{QGP} [112], freeze-out time τ_{fo} at $z = 0$ [16], “comoving” volume $V_{com}(\tau_{fr})$ along the freeze-out surface. V_{Pb} denotes the rest frame size of a lead nucleus. The value $dN_{ch}/dy = 400$ is a measured one [36].

the momentum spectra (NA44, NA49, WA98) of identical particles indicate that the system indeed is an extended one, with a large volume and finite lifetime (sec. 2.4). The pattern of the low-mass e^+e^- enhancement, observed by CERES in S+Au and Pb+Au collisions (sec. 2.7), also strongly lends support to the picture of a collective, thermal, system of hadrons. The observed various pieces of evidence of collectivity alone do not necessarily imply that the system would have reached the QGP phase. The estimated initial energy densities are sufficient (table 1) but the flow studies and the event-by-event measurements of global variables (sec. 2.5) have not shown any dynamical non-trivial fluctuations typical for exotic events.

However, the fact that definite additional anomalies are observed gives more support to the QGP interpretation:

Strangeness production in $A+B$ (sec. 2.6) is globally enhanced (NA35/49, WA97, NA38/50).

Moreover, as observed by WA97, there is a clear specific enhancement of multistrange hadrons: the yield of $\Omega^- + \Omega^+$ per negative hadrons is enhanced by a factor ~ 10 in Pb+Pb collisions relative to p+p and p+Be. Microscopic hadronic rescattering models imply that as multistrange hadrons are difficult to produce due to the high mass-thresholds, the strangeness increase must have an origin at the partonic level, before hadronization. The agreement of the thermal models (sec. 2.3) with the measured hadron abundancies suggests that it is very likely that the system is indeed thermalized already before the completion of hadronization.

Finally, the best candidate for a direct QGP signature so far is the anomalous suppression of J/Ψ observed in central Pb+Pb collisions by NA50 (sec. 2.8). It is very difficult to explain the additional, anomalous, suppression of J/Ψ (i.e. the suppression in addition to the expected suppression in nuclear matter) without invoking partonic degrees of freedom and deconfined matter. I would like to emphasize that in any possible alternative scenario, *all* the previously mentioned features of a collective system and the importance of partonic degrees of freedom will also have to be explained *simultaneously*. To my best knowledge, such an alternative interpretation does not exist so far.

My conclusion of the results from URHIC at the SPS therefore is that collective behaviour of matter is observed but so far there is not yet a 100% certain proof of an observation of the QGP, although the strangeness enhancements and the anomalous J/Ψ suppression strongly suggest it.

4.2. SPS \rightarrow RHIC \rightarrow LHC/ALICE

In increasing the cms-energy of AA -collisions, the quantitative gains are obvious (sec. 3.2): the system becomes initially denser and hotter, it forms faster and stays collective for a longer time, i.e. its lifetime grows and volume increases. The longer the QGP-phase itself can be made, the better chances there are to observe direct QGP signatures.

The higher the cms-energy is, the higher are also the rates for the truly *hard probes* of QGP which cannot be studied at the SPS. At RHIC and LHC/ALICE, these additional QGP probes include Υ (especially its suppression) and open beauty production (at the LHC in particular), jets, high- p_T direct photons, and high mass dileptons. Measurements of Z^0 may also be possible in Pb+Pb collisions at the CMS. At the high energies of RHIC and especially at the LHC/ALICE, the hot initial conditions of the QGP are also expected to become

more reliably calculable based on perturbative QCD.

According to the official plans at the time of this meeting, RHIC at BNL should be in operation in December 1999, so the first exciting data on global variables at high energies will be available in year 2000. A bit further in the future, LHC/ALICE at CERN will start in 2005, completing the extensive experimental program of ultrarelativistic heavy ion collisions. As the URHIC program at the SPS is currently teaching us, at RHIC and ALICE the observation of the QGP will be confirmed by studying carefully *several independent observables simultaneously*. After the results from LHC/ALICE, a broad range of the QCD phase diagram has been experimentally probed, and more light has been shed to the theory of elementary particle condensed matter physics and to the early evolution of our Universe.

Acknowledgements. I thank K. Kajantie, U. Heinz, V. Ruuskanen, J. Schukraft, C. Lourenço, P. Huovinen, V. Kolhinen and K. Tuominen for discussions and help in preparing this talk.

References

- [1] U. Heinz, Proc. *Strong and Electroweak Matter '98*, December 1998, Copenhagen, CERN-TH-99-45, hep-ph/9902424.
- [2] U. Heinz, Proc. *Quark Matter '99*, May 1999, Torino, CERN-TH/99-209, nucl-th/9907060.
- [3] J.-P. Blaizot, Proc. *Quark Matter '99*, SACLAY-SPHT-T99-103, hep-ph/9909434.
- [4] S.A. Bass, M. Gyulassy, H. Stocker and W. Greiner, J. Phys. G25 (1999) R1.
- [5] E. Laermann, Proc. *Quark Matter '96*, Nucl. Phys. A610 (1996) 1c.
- [6] G. Boyd et al, Phys. Rev. Lett. 75 (1995) 4169.
- [7] G. Roland for NA49, Proc. *Quark Matter '97*, Nucl. Phys. A638 (1998) 91c.
- [8] B. Barrois, Nucl. Phys. B129 (1977) 390; D. Bailin and A. Love, Phys. Rept. 107 (1984) 325.
- [9] M. Alford, K. Rajagopal and F. Wilczek, Phys. Lett. B422 (1998) 247; R. Rapp, T. Schäfer, E.V. Shuryak and M. Velkovsky, Phys. Rev. Lett. 81 (1998) 53; R.D. Pisarski and D.H. Rischke, Phys. Rev. Lett. 83 (1999) 37.
- [10] K. Rajagopal, Proc. *Quark Matter 99*, Preprint MIT-CTP-2895, hep-ph/9908360.
- [11] J.D. Bjorken, Phys. Rev. D27 (1983) 140.
- [12] E.L. Feinberg, Nuovo Cimento 34A (1976); E.V. Shuryak, Phys. Lett. B78 (1978) 150; R.C. Hwa and K. Kajantie, Phys. Rev. D32 (1985) 1109; K. Kajantie, J. Kapusta, L. McLerran and A. Mekjian, Phys. Rev. D34 (1986) 2746.
- [13] P.V. Ruuskanen, Proc. *Quark Matter '91*, Nucl. Phys. A544 (1992) 169c.
- [14] J. Wambach and R. Rapp, Proc. *Quark Matter '97*, Nucl. Phys. A638 (1998) 171c.
- [15] H. Satz and X.-N. Wang (eds.), Int. J. Mod. Phys. 10 (1995) 2881.
- [16] K. Kajantie, R. Raitio and P.V. Ruuskanen; Nucl. Phys. B222 (1983) 152; M. Kataja and P.V. Ruuskanen, L. McLerran and H. von Gersdorff, Phys. Rev. D34 2755 (1986) 2755.
- [17] P.V. Ruuskanen, Proc. *Quark Matter '87*, Z. Phys. C38 (1988) 219; K.S. Lee, U. Heinz and E. Schnedermann, Z. Phys. C48 (1990) 525.
- [18] J. Stachel, Proc. *INPC '98*, Nucl. Phys. A654 (1999) 119.
- [19] B. Müller and P. Braun-Munzinger, <http://www.cern.ch/HIPS>.
- [20] I.G. Bearden et al, NA44, Phys. Rev. Lett. 78 (1997) 2080; M. Kaneta for NA44, Proc. *Quark Matter '97*, Nucl. Phys. A638 (1998) 419c; A Sakaguchi for NA44, ibid. 103c.
- [21] F. Pühlhofer for NA49, Proc. *Quark Matter '97*, Nucl. Phys. A638 (1998) 431c.
- [22] H. Appelshäuser et al, NA49, Phys. Lett. B444 (1998) 523.
- [23] E. Andersen et al, WA97, Phys. Lett. B433 (1998) 209; R. Lietava for WA97, Proc. *Strangeness '98*, J. Phys. G: Nucl. Part. Phys. 25 (1998) 345.
- [24] M.M. Aggarwald et al, WA98, Nucl. Phys. A638 (1998) 147c.
- [25] H. van Hecke, H. Sorge and N. Xu, Phys. Rev. Lett. 81 (1998) 5764; A. Dumitru et al, Phys. Lett. B460 (1999) 411.
- [26] Nu Xu for NA44, Proc. *Quark Matter 96*, Nucl. Phys. A610 (1996) 175c.
- [27] J.-Y. Ollitrault, Proc. *Quark Matter '97*, Nucl. Phys. A638 (1998) 195c.
- [28] A.M. Poskanzer and S.A. Voloshin for NA49, Proc. *Quark Matter '97*, Nucl. Phys. A638 (1998) 463c.
- [29] A.M. Poskanzer for NA49, Proc. *Quark Matter '99*, nucl-ex/9906013.
- [30] S. Kabana for NA52, Proc. *Quark Matter '97*, Nucl. Phys. A638 (1998) 411c.
- [31] S. Nishimura for WA98, Proc. *Quark Matter '97*, Nucl. Phys. A638 (1998) 459c; H. Schlagheck for NA98, Proc. *Quark Matter '99*.

- [32] H. Heiselberg and A.-M. Levy, Phys. Rev. C59 (1999) 2716; H. Sorge, Phys. Rev. Lett. 82 (1999) 2048.
- [33] J. Sollfrank, Eur. Phys. J. C9 (1999) 159.
- [34] J. Cleymans and K. Redlich, Phys. Rev. Lett. 81 (1998) 5284.
- [35] P. Braun-Munzinger, Heppe, J. Stachel, nucl-th/9903010, Phys. Lett. B in press.
- [36] P.G. Jones for NA49, Proc. *Quark Matter '96*, Nucl. Phys. A610 (1996) 188c.
- [37] J. Günter, Ph.D. Thesis, Frankfurt (1998) 152. D. Röhrich for NA49, Proc. *International Workshop XXV on Gross Properties of Nuclei and Nuclear Excitations*, Hirschegg (1997) 299.
- [38] F. Gabler, NA49, J. Phys. G: Nucl. Part. Phys. 25 (1999).
- [39] T. Peitzmann for WA98, Proc. *ICHEP98*, Vancouver (1998).
- [40] E. Andersen et al, WA97, J. Phys. G: Nucl. Part. Phys. 25 (1999) 181; CERN-EP/99-29, Phys. Lett. B, in print.
- [41] I. Kralik for WA97, Proc. *Quark Matter '97*, Nucl. Phys. A638 (1998) 115c.
- [42] D. Jouan for NA50, Proc. *Quark Matter '97*, Nucl. Phys. A638 (1998) 483c; A. De Falco for NA50, ibid. 487c.
- [43] J. Rafelski and J. Letessier, nucl-th/9903018.
- [44] R. Hanbury Brown and R.Q. Twiss, Phil. Mag. 45 (1954) 663.
- [45] U. Heinz, Proc. *Quark Matter '96*, Nucl. Phys. A610 (1996) 264c.
- [46] S. Pratt, Proc. *Quark Matter '97*, Nucl. Phys. A638 (1998) 125c.
- [47] U.A. Wiedemann, Proc. *Quark Matter '99*, nucl-th/9907048.
- [48] U.A. Wiedemann and U. Heinz, CU-TP-931, nucl-th/9901094, Phys. Rept. 319 (1999) 145.
- [49] E. Shuryak, Phys. Lett. B44 (1973) 387; M. Gyulassy, S.K. Kauffmann and L.W. Wilson, Phys. Rev. C20 (1979) 22267; S. Pratt, Phys. Rev. Lett. 53 (1984) 1219.
- [50] A. Franz for NA44, I.G. Bearden et al, Proc. *Quark Matter '96*, Nucl. Phys. A610 (1996) 240c.
- [51] R. Ganz for NA49, MPI-PHE-99-12, Proc. *Quark Matter '99*, nucl-ex/9909003; H. Appelshauser et al, NA49, Eur. Phys. J. C2 (1998) 661.
- [52] I.G. Bearden for NA44, Proc. *Quark Matter '99*.
- [53] S. Vörös for WA98, Proc. *Quark Matter '99*.
- [54] J. Randrup, Proc. *Quark Matter '97*, Nucl. Phys. A638 (1998) 439c.
- [55] F. Siklér for NA49, Proc. *Quark Matter '99*.
- [56] G. Odyniek, Proc. *Quark Matter '97*, Nucl. Phys. A638 (1998) 135c.
- [57] Proc. *Strangeness in Quark Matter '98*, July 1998, Padova, J. Phys. G25 (1998) 143-484.
- [58] M. Gaździcki et al, NA35, Nucl. Phys. A498 (1989) 375.
- [59] F. Becattini, M. Gaździcki and J. Sollfrank, Eur. Phys. J. C5 (1998) 143.
- [60] T. Alber et al, NA35, Z. Phys. C64 (1994) 195; Preprint IKF-HENPG/6-94; Phys. Lett. B366 (1996) 56; J. Bächler et al, NA35, Z. Phys. C58 (1993) 367.
- [61] V. Friese et al., NA49, J. Phys. G23 (1997) 1837; C. Bormann et al, NA49, ibid. 1817; I. Huang, Ph.D. Thesis, NA49, U.C. Davis (1997).
- [62] F. Antinori for WA97, Proc. *Quark Matter '99*.
- [63] D. Elia for WA97, Proc. *Quark Matter '99*.
- [64] C. Höhne for NA49, Proc. *Quark Matter '99*.
- [65] N. Willis for NA50, Proc. *Quark Matter '99*.
- [66] A. Białas, Phys. Lett. B442 (1998) 449; J. Zimányi, T. Biró and P. Lévai, hep-ph/9904501.
- [67] P. Wurm for NA45/CERES, Proc. *Quark Matter '95*, Nucl. Phys. A590 (1995) 103c.
- [68] G. Agakichiev et al, CERES, Phys. Rev. Lett. 75 (1995) 1272.
- [69] M. Masera for HELIOS-3, Proc. *Quark Matter '95*, Nucl. Phys. A590 (1995) 93c.
- [70] De Falco for NA38, Proc. *Quark Matter '97*, Nucl. Phys. A638 (1998) 487c.
- [71] I. Tserrya, Proc. *Quark Matter '95*, Nucl. Phys. A590 (1995) 127c.
- [72] I. Tserrya, Proc. *Quark Matter '97*, Nucl. Phys. A638 (1998) 365c.
- [73] B. Lenkeit for CERES, Proc. *Quark Matter '99*, nucl-ex/9910015.
- [74] G. Agakichiev et al, CERES, Eur. Phys. J C4 (1998) 231.
- [75] R. Rapp, Proc. *Quark Matter '99*, SUNY-NTG-99-24, hep-ph/9907342.
- [76] G.Q. Li, C.M. Ko and G.E. Brown, Phys. Rev. Lett 75 (1995) 4007.
- [77] P. Huovinen and M. Prakash, Proc. *Quark Matter '99*, nucl-th/9907064; Phys. Lett. B450 (1999) 15.
- [78] J. Sollfrank et al, Phys. Rev. C55 (1997) 392; P. Huovinen, P.V. Ruuskanen and J. Sollfrank, Nucl. Phys. A650 (1999) 227.
- [79] J.V. Steele, H. Yamagishi and I. Zahed, Phys. Lett. B384 (1997) 255; Phys. Rev. D56 (1997) 5605; R. Rapp, M. Urban, M. Buballa and J. Wambach, Phys. Lett. B417 (1998) 1.

- [80] S. Ramos for NA38, Proc. *Quark Matter '95*, Nucl. Phys. A590 (1995) 117c; C. Lourenço, Universidade Tecnica de Lisboa, Doctoral thesis (1995).
- [81] E. Scapparini for NA50, Proc. *Quark Matter '96*, Nucl. Phys. A610 (1996) 331c; P. Bordalo for NA50, Proc. *Quark Matter '99*.
- [82] P. Huovinen, P.V. Ruuskanen and J. Sollfrank, Proc. *Quark Matter '97*, Nucl. Phys. A638 (1998) 503c.
- [83] M. Gonin for NA50, Proc. *Quark Matter '96*, Nucl. Phys. A610 (1996) 404c.
- [84] M.C. Abreu et al, NA50, Phys. Lett. B410 (1997) 337.
- [85] L. Ramello, Proc. *Quark Matter '97*, Nucl. Phys. A638 (1998) 261c.
- [86] M.C. Abreu et al, NA50, Phys. Lett. B450 (1999) 456.
- [87] C. Cicalò for NA50, Proc. *Quark Matter '99*.
- [88] T. Matsui and H. Satz, Phys. Lett. B178 (1996) 416.
- [89] D. Kharzeev, Proc. *Quark Matter '97*, Nucl. Phys. A638 (1998) 279c.
- [90] R. Vogt, Phys. Rept. 310 (1999) 197.
- [91] H. Satz, Proc. *Quark Matter '99*, hep-ph/9908339.
- [92] M.C. Abreu et al, NA51, Phys. Lett. B 438 (1998) 35; M.C. Abreu et al, NA38, Phys. Lett. B 444 (1998) 516; M.C. Abreu et al, NA38, Phys. Lett. B 449 (1999) 128; M.C. Abreu et al, NA38, CERN-EP/99-113, to appear in Phys. Lett. B.
- [93] K.J. Eskola, V.J. Kolhinen and P.V. Ruuskanen, Nucl. Phys. B535 (1998) 351, hep-ph/9802350; K.J. Eskola, V.J. Kolhinen and C.A. Salgado, Eur. Phys. J. C9 (1999) 61, hep-ph/9807297.
- [94] A. Capella et al, Phys. Lett. B (1988) 354; C. Gerschel and J. Hüfner, Phys. Lett. B 207 (1988) 253; Z. Phys. C 56 (1992) 391.
- [95] S. Gavin, M. Gyulassy and A. Jackson, Phys. Lett. B 207 (1988) 194; R. Vogt, M. Prakash, P. Koch and T.H. Hansson, Phys. Lett. B 207 (1988) 257; S. Gavin and R. Vogt, Nucl. Phys. B345 (1990) 104.
- [96] D. Kharzeev, C. Lourenço, M. Nardi and H. Satz, Z. Phys. C74 (1997) 307.
- [97] F. Karsch, M.T. Mehr and H. Satz, Z. Phys. C37 (1988) 617; F. Karsch and H. Satz, Z. Phys. C51 (1991) 209; S. Gupta and H. Satz, Phys. Lett. B283 (1992) 439.
- [98] D. Kharzeev, Proc. *Quark Matter '96*, Nucl. Phys. A610 (1996) 418c.
- [99] C.-Y. Wong, Proc. *Quark Matter '96*, Nucl. Phys. A610 (1996) 434c; Phys. Rev. C55 (1997) 2621.
- [100] J.-P. Blaizot and J.-Y. Ollitrault, Proc. *Quark Matter '96*, Nucl. Phys. A610 (1996) 452c; Phys. Rev. Lett. 77 (1996) 1703.
- [101] N. Armesto, M.A. Braun, E.G. Ferreira and C. Pajares, Phys. Rev. Lett. 77 (1996) 3736.
- [102] D. Kharzeev, H. Satz, A. Syamtomov and G. Zinovjev, Eur. Phys. J. C9 (1999) 459.
- [103] P. Hoyer and S. Peigne, Phys. Rev. D57 (1998) 1864; Phys. Rev. D59 (1999) 034011.
- [104] RHIC Machine Commissioning Status, <http://www.rhic.bnl.gov>
- [105] J.W. Harris, "Relativistic heavy ion physics and the relativistic heavy ion collider," YRHI-98-13, Lake Louise Winter Institute: QCD, Lake Louise, 1998.
- [106] Conceptual Design Report for the Solenoidal Tracker At RHIC, The STAR Collaboration, PUB-5347 (1992); J.W. Harris et al, Nucl. Phys. A 566 (1994) 277c; <http://www.rhic.bnl.gov/star/starlib/doc/www/star.html>
- [107] PHENIX Experiment at RHIC - Preliminary Conceptual Design Report, PHENIX Collaboration Report (1992); <http://www.phenix.bnl.gov/>
- [108] Interim Design report for the BRAHMS Experiment at RHIC, BNL Report (1994); <http://www.rhic.bnl.gov/export1/brahms/WWW/brahms.html>
- [109] RHIC Letter of Intent to Study Very Low p_T Phenomena at RHIC, PHOBOS Collaboration (1991); <http://www.phobos-srv.lns.mit.edu/>
- [110] ALICE Technical Design report <http://www.cern.ch/ALICE/>
- [111] J.P. Blaizot and A.H. Mueller, Nucl. Phys. B289 (1987) 847; K. Kajantie, P.V. Landshoff and J. Lindfors, Phys. Rev. Lett. 59 (1987) 2527. K.J. Eskola, K. Kajantie and J. Lindfors, Nucl. Phys. B323 (1989) 37.
- [112] K.J. Eskola, K. Kajantie, P.V. Ruuskanen and K. Tuominen, JYFL-8-99, hep-ph/9909456.
- [113] K. Tuominen and K.J. Eskola, in preparation; see also A. Leonidov and D. Ostrovsky, FIAN-TD-24-98, hep-ph/9811417.
- [114] L. McLerran and R. Venugopalan, Phys. Rev. D49 (1994) 2233; A. Krasnitz and R. Venugopalan, hep-ph/9909203 and refs. therein.
- [115] P. Braun-Munzinger, Proc. *Quark Matter '99*, nucl-th/9908007.
- [116] M. Gyulassy and X.-N. Wang, Nucl. Phys. B420 (1994) 583; X.-N. Wang, M. Gyulassy and M. Plumer, Phys. Rev. D51 (1995) 3436; R. Baier, Yu.L. Dokshitzer, A.H. Mueller and S. Peigne, Nucl. Phys. B478 (1996) 577; Nucl. Phys. B484 (1997) 265; Phys. Rev. C60 (1999) 064902.

- [117] M. Gyulassy, P. Lévai and I. Vitev,
hep-ph/9907461, hep-ph/9907343.
- [118] X.-N. Wang, Z. Huang and I. Sarcevic, Phys.
Rev. Lett. 77 (1996) 231.
- [119] R. Vogt, B.V. Jacak, P.L. McGaughey and
P.V. Ruuskanen, Phys. Rev. D49 (1994) 3345;
S. Gavin, P.L. McGaughey, P.V. Ruuskanen
and R. Vogt, Phys. Rev. C54 (1996) 2606;
hep-ph/9604369; K. Gallmeister, B. Kämpfer,
O.P. Pavlenko, Phys. Rev. C57 (1998) 3276.